# VARIATIONS IN MICROSTRUCTURE AND MECHANICAL PROPERTIES OF CAST ALUMINIUM EN AC 43100 ALLOY

**Salem Seifeddine, Torsten Sjögren and Ingvar L Svensson**
**Jönköping University, School of Engineering, Component technology - Sweden**

## Abstract

The microstructure and mechanical properties of a gravity die and sand cast Al-10%Si-0.4%Mg alloy, which is one of the most important and frequently used industrial casting alloys, were examined. Tensile test samples were prepared from fan blades and sectioned through three positions which experienced different cooling rates. Furthermore, the inherent strength potential of the alloy was revealed by producing homogeneous and well fed specimens with a variety of microstructural coarseness, low content of oxide films and micro-porosity defects, solidified in a laboratory environment by gradient solidification technology. The solidification behaviour of the alloy was characterized by thermal analysis. By means of cooling curves, the solidification time and evolution of the microstructure was recorded. The relation between the microstructure and the mechanical properties was also assessed by using quality index-strength charts developed for the alloy. This study shows that the microstructural features, especially the iron-rich needles denoted as β-$Al_5FeSi$, and mechanical properties are markedly affected by the different processing routes. The solidification rate exerts a significant effect on the coarseness of the microstructure and the intermetallic compounds that evolve during solidification, and this directly influences the tensile properties.

## Riassunto

In questo lavoro sono state esaminate la microstruttura e le proprietà meccaniche di una delle leghe più comuni nell'industria delle leghe leggere, la lega Al-10%Si-0.4%Mg, colata per gravità sia in conchiglia che in sabbia. Le provette di trazione sono state ricavate da pala di ventilatore e sono state sezionate in tre posizioni caratterizzate da diverse velocità di raffreddamento. Inoltre è stato valutato il valore potenziale di resistenza a trazione ottenibile della lega, mediante produzione di campioni caratterizzati da diversa morfologia strutturale, basso contenuto di film ossidi microporosità, solidificati in ambiente controllato con metodologia di solidificazione a gradiente. Il comportamento in solidificazione è stato caratterizzato mediante analisi termica. Per mezzo di curve di raffreddamento, si è determinato il tempo di solidificazione e l'evoluzione della microstruttura. La relazione tra la microstruttura e le proprietà meccaniche è stata determinata usando specifiche carte di correlazione indice di qualità – resistenza. Questo studio dimostra che le caratteristiche microstrutturali, in particolare i grani aciculari ad alto tenore di ferro indicati come β-Al5FeSi, e le proprietà meccaniche sono marcatamente condizionate dai differenti percorsi preparativi. La velocità di raffreddamento esercita una significativa influenza sulla morfologia microstrutturale e sui componenti intermetallici che si sviluppano durante la solidificazione, influenzando così direttamente le proprietà di resistenza a trazione.

## KEYWORDS

Aluminium cast alloys, gravity- and sand casting, gradient solidification technique, thermal analysis, porosity, quality index.

## INTRODUCTION

The mechanical properties of cast aluminium alloys are very sensitive to composition, metallurgy and heat treatment, the casting process and the formation of defects during mould filling and solidification. The coarseness of the microstructure and the type of phases that evolve during solidification are fundamental in affecting the mechanical behaviour of the material. The mechanical properties obtained from gradient solidified samples are assumed to represent the upper performance limits of a particular alloy, due to the low level of defects obtained from the favourable melting and solidification procedure.

Different processing routes offer different qualities and soundness of commercial components. The true potential of most alloys is seldom approached, and there exists a lack of data in the literature describing the variations in microstructure and related mechanical properties of alloy EN AC 43100. The present investigation was therefore carried out in order to elucidate and assess the influence of the casting process and resultant variations of microstructure on the mechanical properties, by extracting tensile specimens from Al-10%Si-0.4%Mg commercial cast components manufactured by two different casting methods; sand and gravity die casting. In addition, the inherent strength potential of this casting alloy will be investigated by manufacturing tensile test specimens using gradient solidification technology. The mechanical properties which have been measured in this work are: ultimate tensile strength, yield strength and fracture elongation. The microstructural features that have been evaluated are the secondary dendrite arm spacing (SDAS), pore fraction and precipitated phases such as the length of the iron-rich β-phase, $Al_5FeSi$.

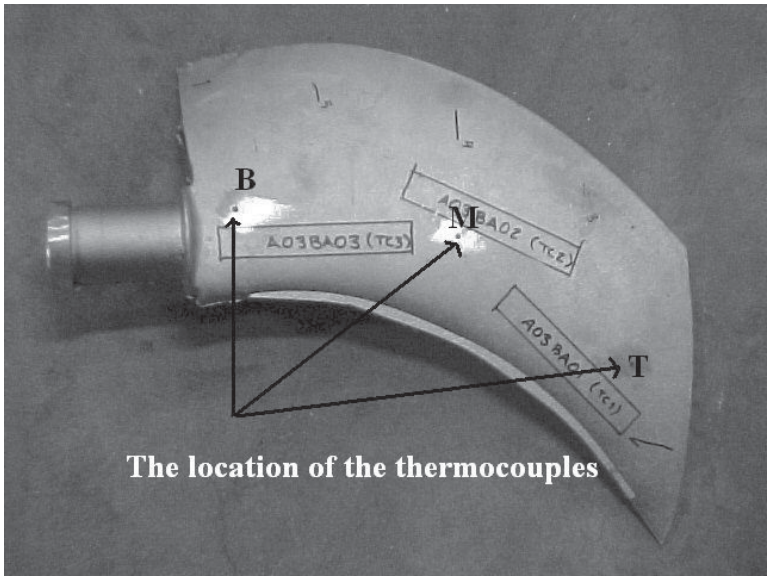


Fig. 1: Fan blade cast in sand- and gravity moulds.

## MATERIALS AND EXPERIMENTS

### Cast component

The components that have been studied are fan blades, as shown in figure 1, which are produced commercially in a great variety of shapes and sizes, and by different casting methods. This particular component is considered to be of interest to study and analyse due to the widespread use of different casting methods to manufacture fan blades, which in this case were manufactured by sand mould- and gravity die casting.

The locations of the specimens extracted for study are shown in figure 1; from the top (T), middle (M) and bottom (B) parts of the fan blade. These locations were chosen due to their different solidification times (i.e. thicknesses), which results in different coarseness of the microstructure, intermetallic phases and defects.

### Cast alloy

The commercial blades and specimens produced by gradient solidification experiments were cast using alloy EN AC 43100. The standard composition of the alloy and the actual composition are given in table 1. Strontium was

Table 1: Chemical composition of the casting alloy

| Composition | | Elements (wt. %) | | | | | | | | | |
|---|---|---|---|---|---|---|---|---|---|---|---|
| Alloy | Standard | Si | Fe | Cu | Mn | Mg | Zn | Ti | Cr | Ni | Al |
| EN AC-43100 | SS-EN 1706 | 9.0-11.0 | 0.55 | 0.10 | 0.45 | 0.20-0.45 | 0.10 | 0.15 | - | 0.05 | Bal. |
| EN AC-43100 | Actual sample | 9.96 | 0.47 | 0.11 | 0.25 | 0.35 | 0.097 | 0.018 | 0.01 | 0.01 | Bal. |

added in the form of Al-10%Sr master alloy at a level of 150- 200 ppm.

### Sand and gravity die casting

The sand moulds used were made by hand. As a pattern, a fan blade cast in a gravity mould was used, which is as already mentioned, one of the methods normally used to manufacture this size and type of fan blade. The sand mould consisted of chemical bonded sand.

### Gradient solidification

The same alloy as that used for the sand and gravity die cast components, shown in table 1, was cast into rods for further solidification studies in the gradient solidification equipment. The gradient solidification technique allows the production of a high quality material with a low content of oxide films, porosity and shrinkage related defects, and produces a homogenous and well-fed microstructure throughout the entire specimen. In this work a resistance-heated furnace with an electrically driven elevator was used, see figure 2a. Three different growth velocities, *v*, were used, 0.03 mm/s, 0.3 mm/s and 3 mm/s, which correspond respectively to an SDAS of about 50, 20 and 7 μm. At each velocity, three specimens were made. The specimens cast in the gradient solidification equipment were protected by argon in order to avoid oxidation.

### Thermal analysis

In order to study the thermal history of the solidified components, thermocouples were inserted at three different positions in the sand cast fan blade, as indicated in the picture in figure 1. To record the cooling curves a data acquisition device from National Instruments was used. In each of the sand moulds three thermocouples were placed. The thermocouples were of S-type, which means that the different materials in the thermocouple wires are platinum and platinum-rhodium (90Pt-10Rh). When manufacturing the thermocouples, the wires are inserted in a two-hole $Al_2O_3$-tube to separate the wires, which are connected to a plug. The thermocouples were protected from the molten metal by a quartz glass tube. The maximum operating temperature for the S-type thermocouple is over 1500°C [1]. The recording rig is illustrated in figure 2b.

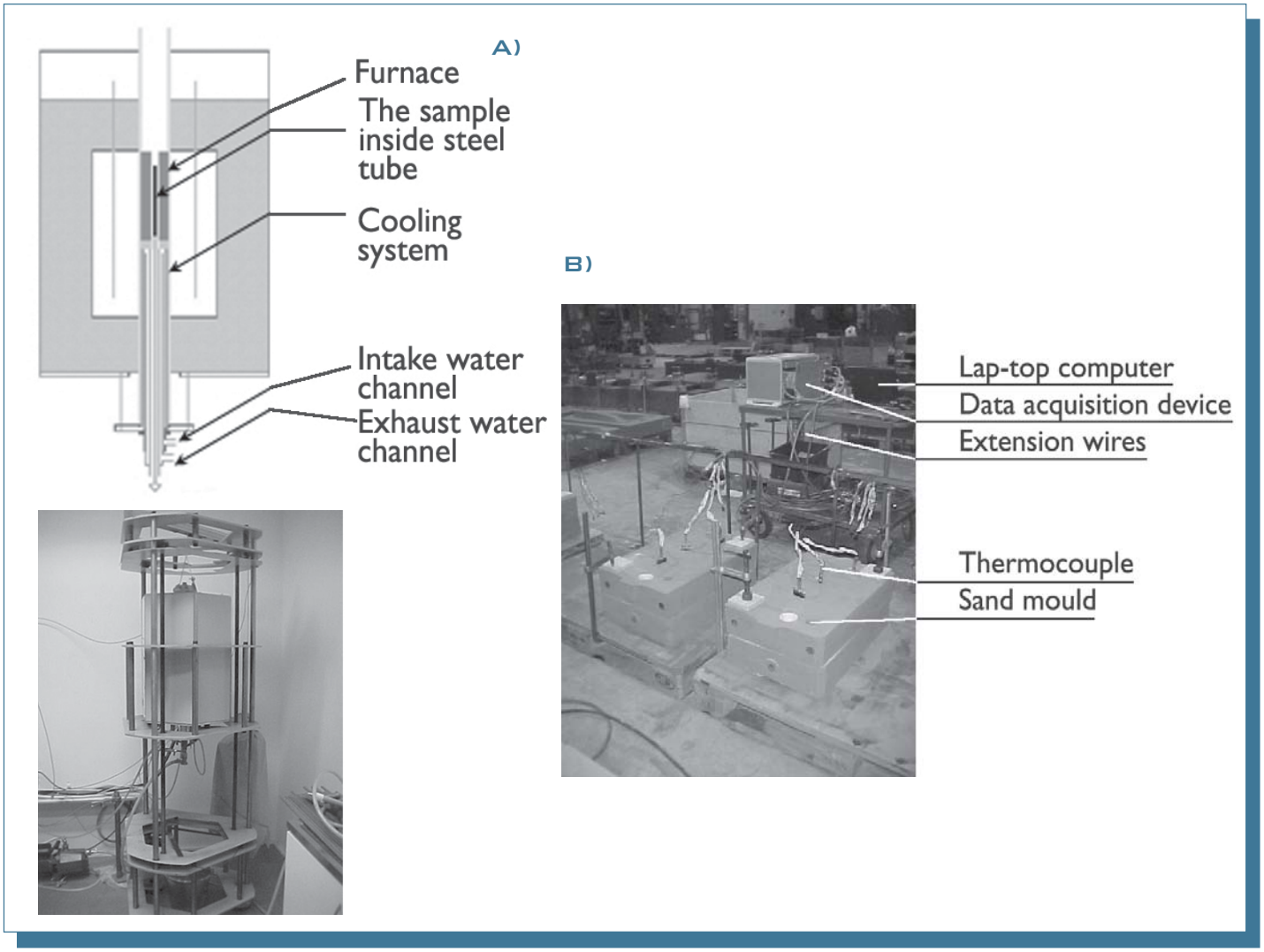


Fig. 2: . *Illustration of the instruments that have been used during the investigation. While a) demonstrates the gradient solidification equipment, b) presents the data acquisition rig that is connected to the sand moulds.*

## RESULTS OF THE MICROSTRUCTURE AND MECHANICAL PROPERTIES INVESTIGATION

Since specimens were extracted from fan blades with different thickness and at different sections it was necessary to machine them in order to obtain specimens suitable for tensile testing. The gradient solidified specimens have also been prepared in the same manner, and the dimensions of the samples used for tensile testing are shown in figure 3. In order to analyse the microstructure and measure the different microstructural features, a light microscope, image processing software and a scanning electron microscope, SEM, were used.

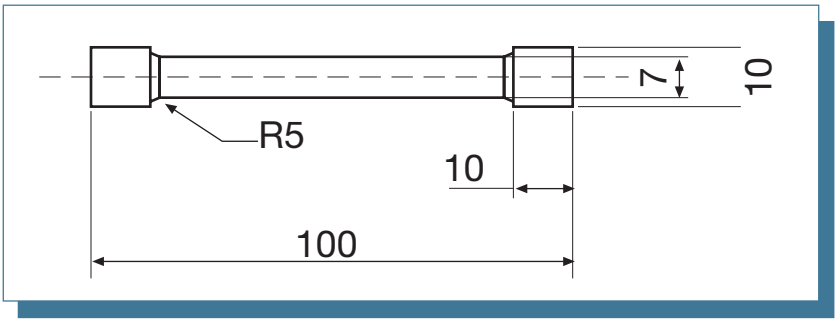


Fig. 3: A schematic illustration of the tensile specimen (dimensions in mm).

### Microstructure development

The microstructure coarseness is defined as the secondary dendrite arm spacing, SDAS, which is also a function of the local solidification time, and quantifies the scale of the microstructure and its constituents. Examining the microstructure of specimens from both sand and gravity die casting, it has been observed that there is a wide scattering of SDAS and consequently variations of sizes and shapes of the intermetallic compounds within the same component. The needle-shaped β-phase, $Al_5FeSi$ also seems to coexist with the α-phase, $Al_{15}(Fe,Mn)_3Si_2$, which has the morphology of Chinese script. As depicted in figure 4, the dendrites are equiaxed and the eutectic is finely modified. Comparing the microstructure formations, it can be noticed that in the case of gravity die casting the microstructure is finer, due to the higher cooling rate. Furthermore, the different coarsenesses of microstructure, the phases and their morphologies are comparable to the sand cast microstructure.

It is relevant to note that even if Mn has been added to the alloy to act as an Fe-corrector and to promote the formation of Chinese script, see table 1, iron-rich $Al_5FeSi$-needles are still formed. These needles act as local stress raisers in the matrix and are considered to be deleterious for the mechanical performance, which is why their formation and growth should be taken into consideration and as much as possible suppressed.

In order to understand the local variations in microstructure, and to understand the formation sequences and development of constituent phases in the sand cast component, thermal analysis was implemented. When manufacturing the sand cast fan blades at the foundry, data for the cooling curves was recorded. In each of the sand moulds, three thermocouples were used, as shown in figure 1.

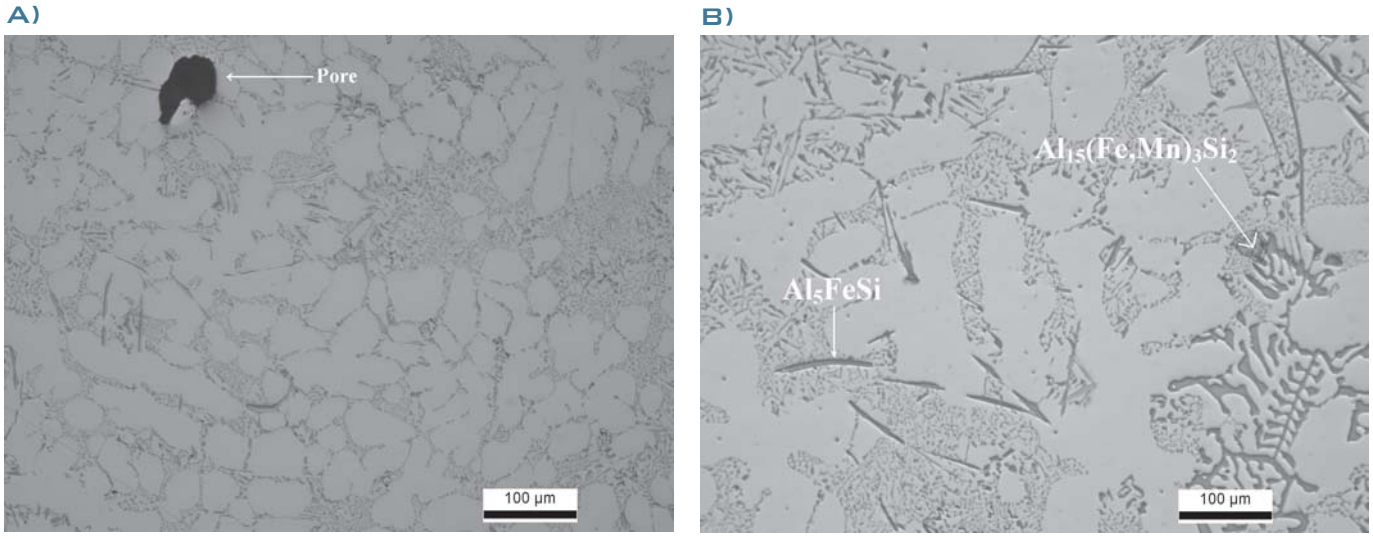


Fig. 4: . a) Illustration of the microstructure of a gravity die cast specimen while b) shows a sand cast microstructure. The black spot is a pore.

With this composition, see table 1, and casting technique, three different cooling curves have been obtained and are presented in figure 5a. The figure also shows that there exists clear variations in local solidification times which are directly related to the variations in component thickness, see also table 2. These variations in cooling time lead to major local differences in microstructures which affect the tensile performance of the cast components. The SDAS for the sand cast and gravity die cast component varied between 47-61 μm and 20-45 μm respectively.

Figure 5b shows that the freezing range is approximately between 595°C and 545°C. From the different cooling curves it is possible to see at which temperature and time the dendritic network starts to grow, at which temperature and time the eutectic starts to grow and also the total solidification time, from pouring the melt until the fraction solid has reached 100%.

When the value of the derivative exceeds zero, figure 5b, the temperature is actually increasing due to the release of latent heat due to phase transformations. This is most evident in the case where a positive derivative is observed at about 590°C when the dendritic network starts to grow. The next positive value of the derivative appears when the eutectic starts to grow, at about 570°C. When the temperature is around 550°C precipitations of a complex eutectic with intermetallics and a hardening phase such as $Mg_2Si$ starts to precipitate from the remaining melt. From the different thermocouples the following solidification times have been determined:

Table 2. Solidification times for the different parts of the sand cast fan blade.

| Thermocouple | Thinnest part (T) | Mid part (M) | Bottom part (B) |
|---|---|---|---|
| Solidification time (s) | 260 | 470 | 610 |
| Material thickness (mm) | 12 | 20 | 28 |

Examining the gradient solidified specimens, a significant discrepancy between the different solidification rates is observed. The higher the cooling rate the finer the microstructure, as illustrated in figure 6. The iron-rich β-phase $Al_5FeSi$ is found to be very short and very well dispersed for the two highest solidification velocities; 3 and 0.3 mm/s, with a corresponding SDAS ≈ 7 and 23 μm respectively, in comparison to the lowest velocity 0.03 mm/s, with SDAS ≈ 47 μm, where long iron-bearing phases were found randomly distributed in the eutectic regions.

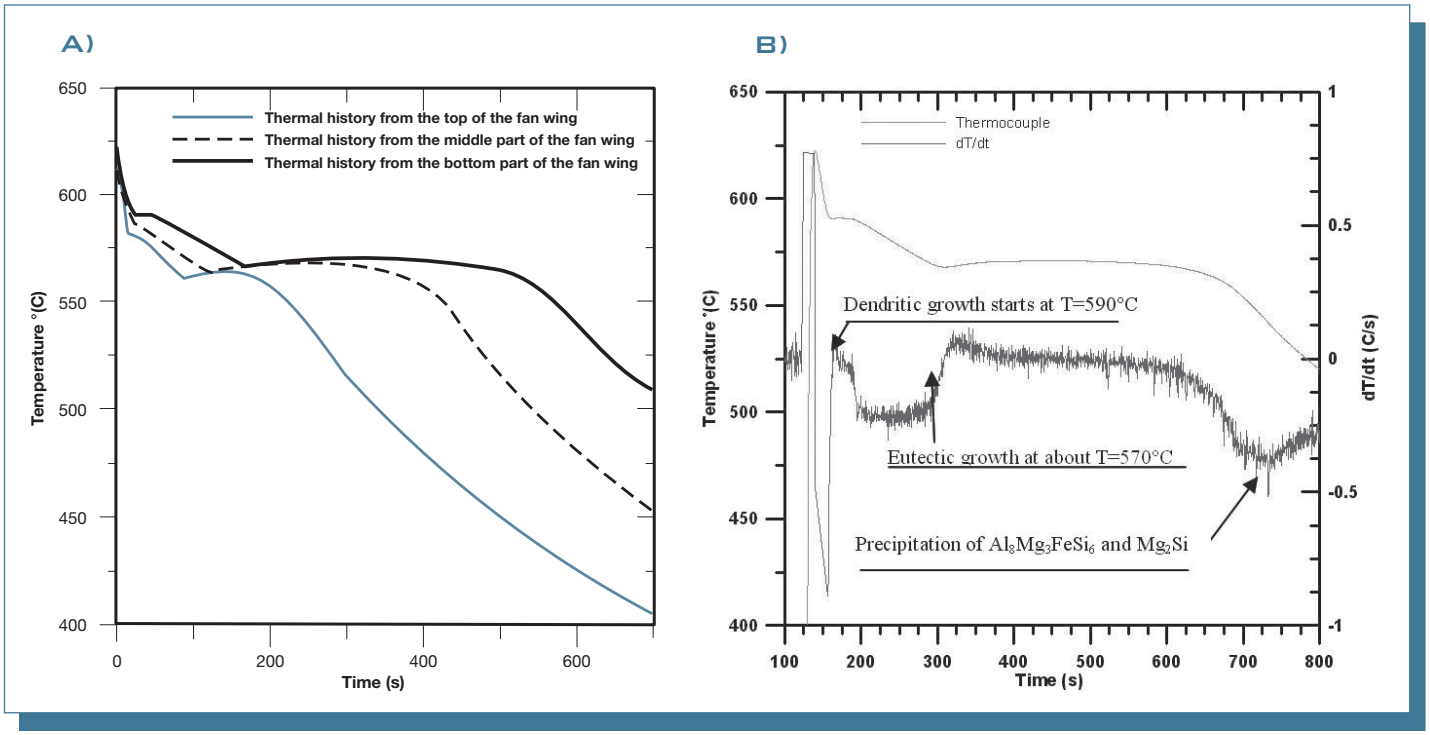


Fig. 5: The thermal history of the sand cast component is registered in figure a) while in b) an analysis of the cooling curve obtained from the bottom section is performed.

## Mechanical properties

The results of the tensile tests from the commercial fan blades and the laboratory prepared samples are shown in the diagrams in figure 7. The two different casting methods are compared in figure 7a, where each point represents a different position on the fan blade. A wide scatter in data is clearly observed but it can be noticed that the properties of the thinner parts seem to approach higher combinations of stress and strain values.

In order to simulate the processes of the cast components, tensile test samples of the same alloy and corresponding microstructural coarseness have been produced by using gradient solidification. By producing a more homogenous microstructure with a lower level of defects, the material's inherent potential was revealed, see figure 7b. The scatter in data in figure 7b is ascribed to different levels of defects, and the higher stress-strain combinations are the limits for what this alloy might perform under ideal conditions.

When quantifying the SDAS, five measurements were taken at three randomly chosen positions of the specimen. From these data a mean value was calculated. At high solidification rates the SDAS

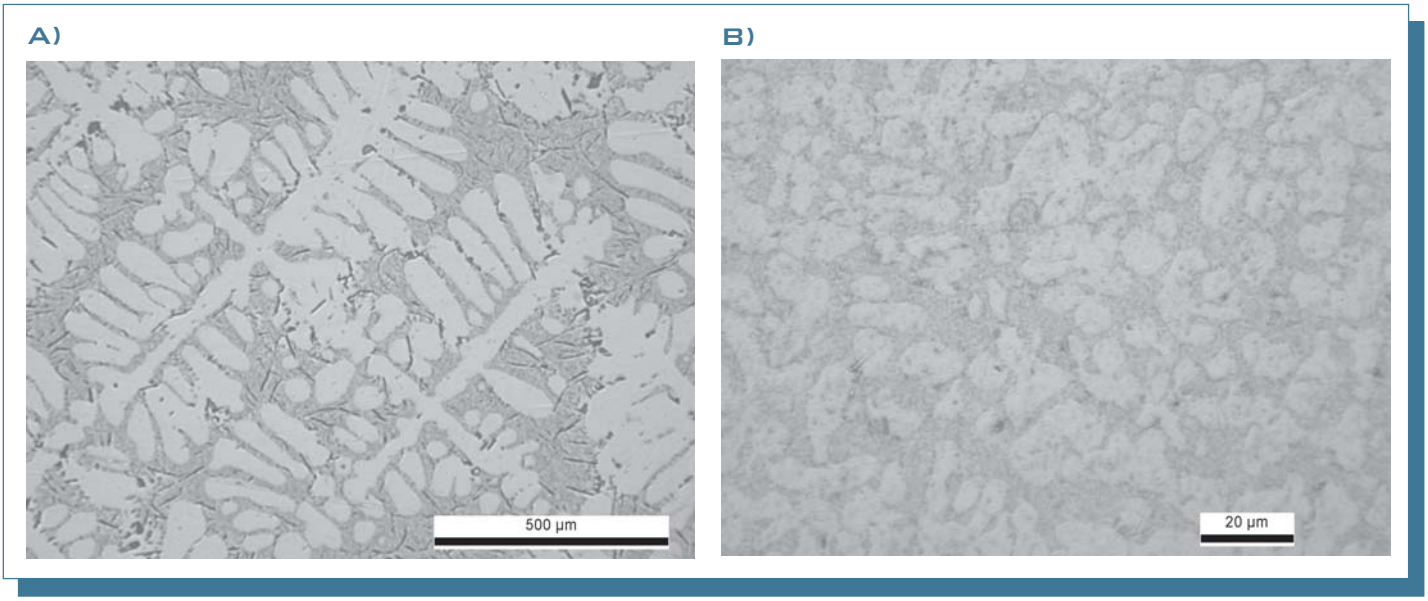


Fig. 6: Phases and microstructures for a) SDAS = 47 µm obtained at 0.03 mm/s and b) SDAS = 7 µm obtained at 3 mm/s.

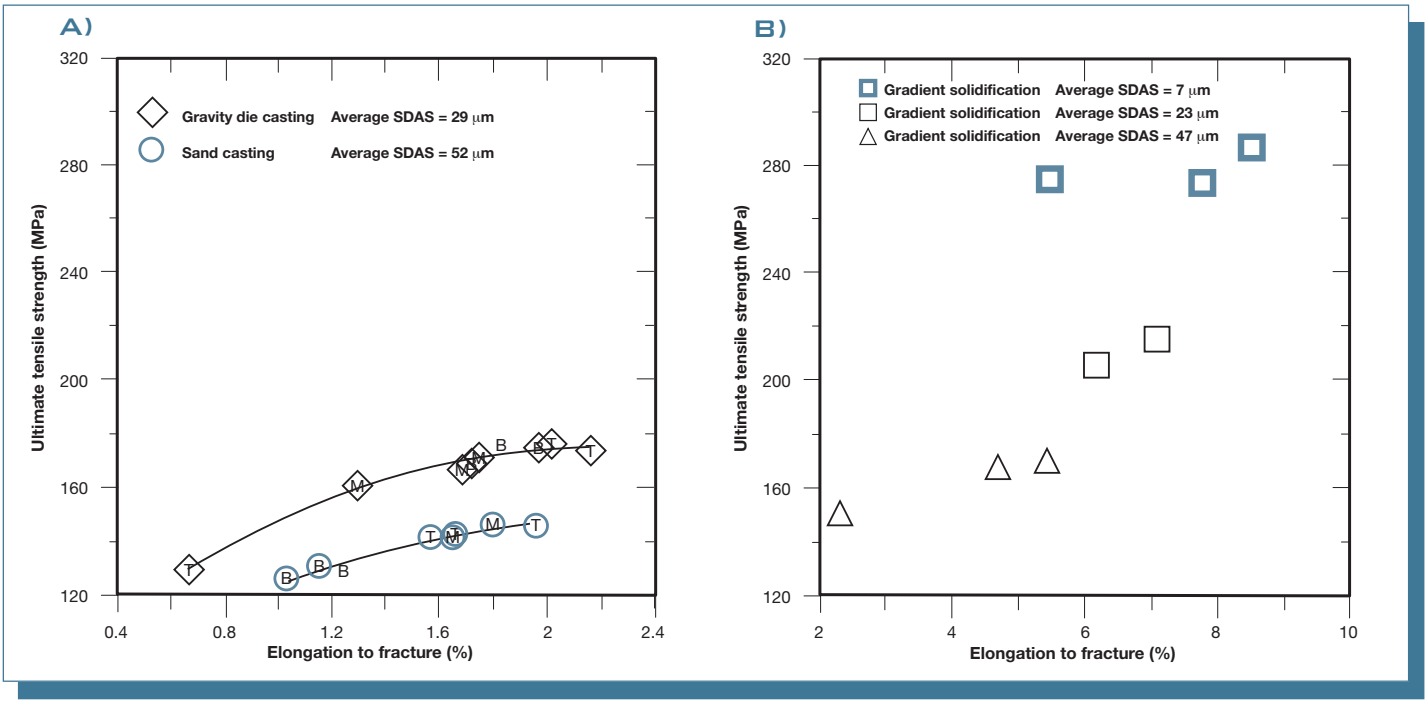


Fig. 7: The graph in a) illustrates the ultimate tensile strength and elongation to fracture for the gravity die and sand casting specimens where B is the bottom (thickest) section, M the middle and T the top (thinnest) part of the blade. The graph in b) presents the tensile properties for the gradient solidified specimens with a range of cooling rates.

appears to be very small and the microstructure has been found to be more uniform. As noticed, the overall effect of obtaining a small SDAS is an improvement in both ductility and tensile strength, see figure 8.

When measuring the length of the iron-rich $Al_5FeSi$ needles (β-phase), the 15 longest needles observed in the microstructure were measured, considering the entire cross-section area of the sample, and a mean value was assessed. It should be mentioned that the needles were not chemically analyzed, but were identified according to their morphologies and colours. A correlation was found between the length of the β-phase and the mechanical properties. An increase in needle length results in a reduction of tensile strength and elongation as can be seen in figure 9. Note that the iron-bearing β-phase was too short to be measured or not present at all in the specimen solidified at a rate of 3 mm/s, SDAS = 7 μm. It is also seen that even if these needles are relatively shorter in some cases than in corresponding samples, they exhibited lower properties. The premature fractures must therefore be due to other defects such as oxide film inclusions or other brittle and undesirable phases such as $Al_8Mg_3FeSi_6$. These intermetallics are harmful to the mechanical properties since cracking of these phases reduces the ductility,

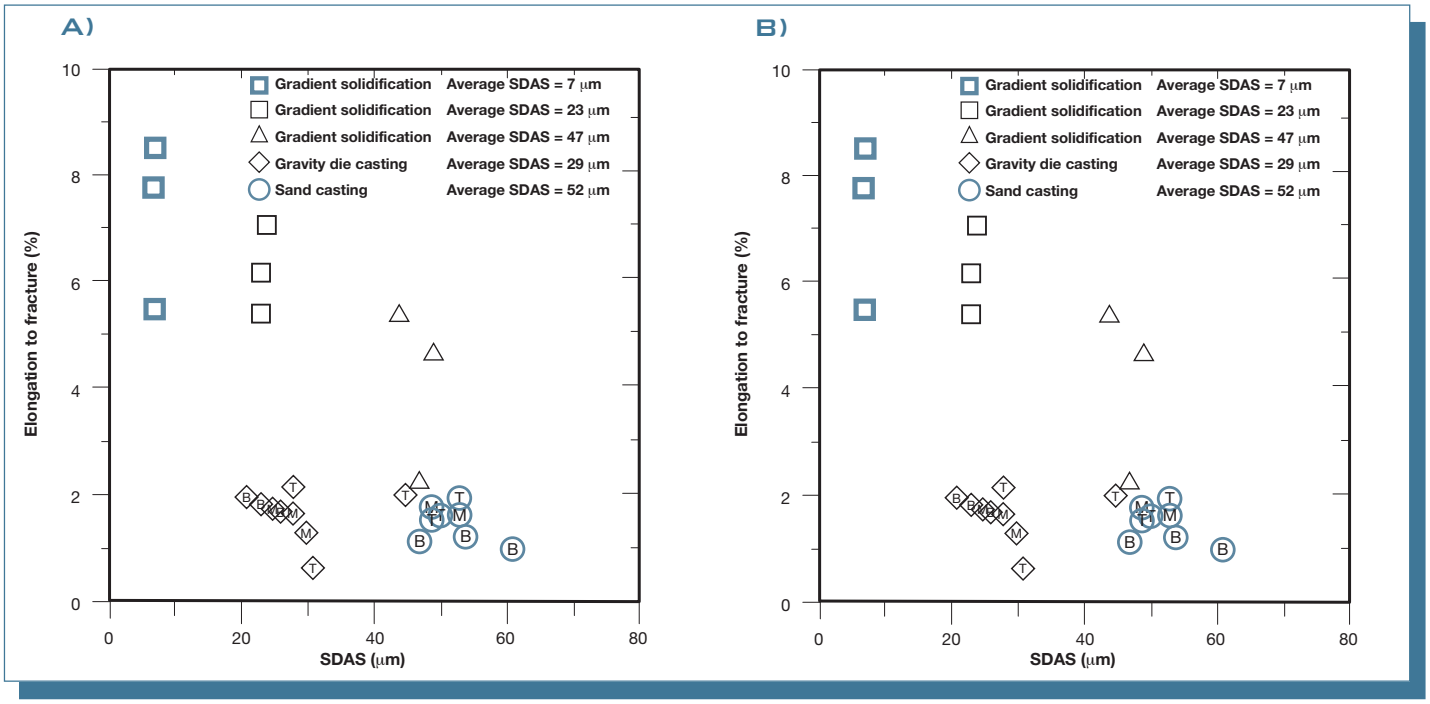


Fig. 8: The graphs a) and b) illustrate the influence of SDAS on the tensile properties.

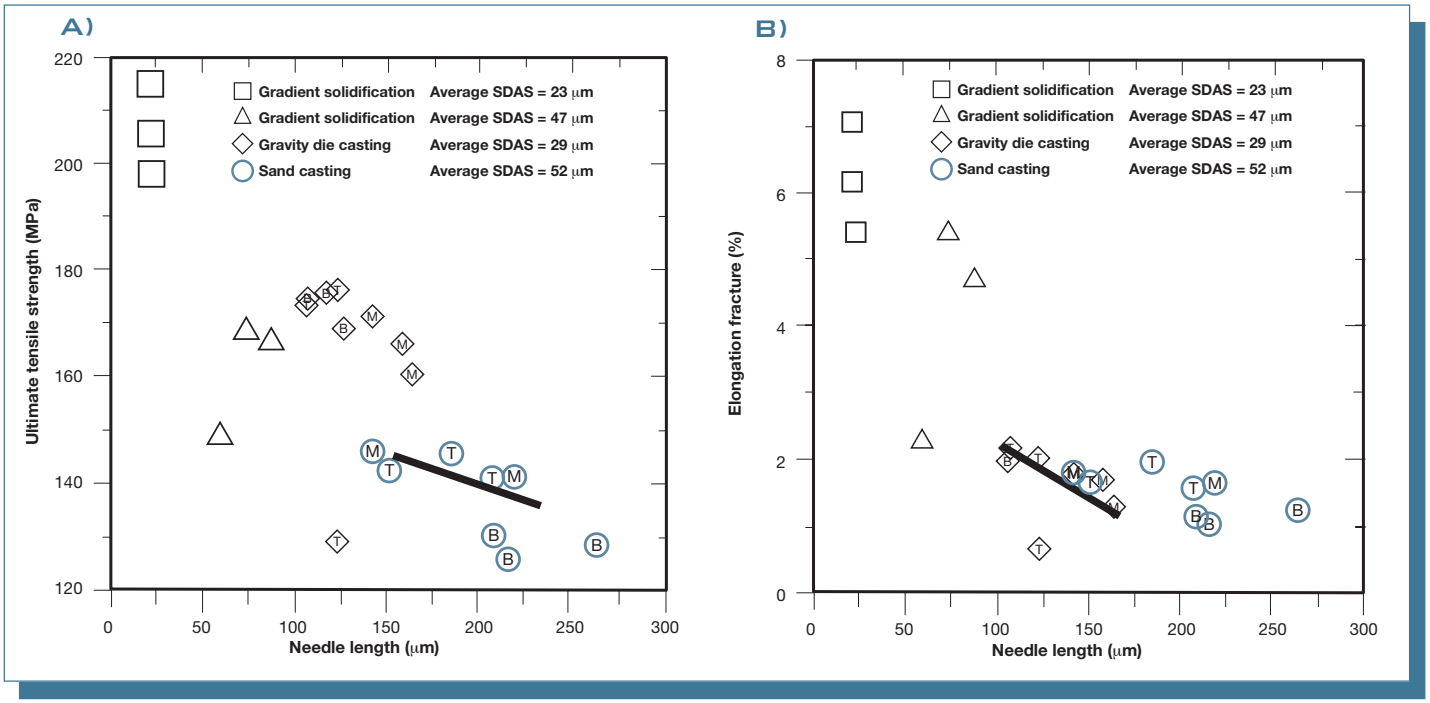


Fig. 9: The influence of the β-phase needle length on a) ultimate tensile strength and b) the elongation to fracture.

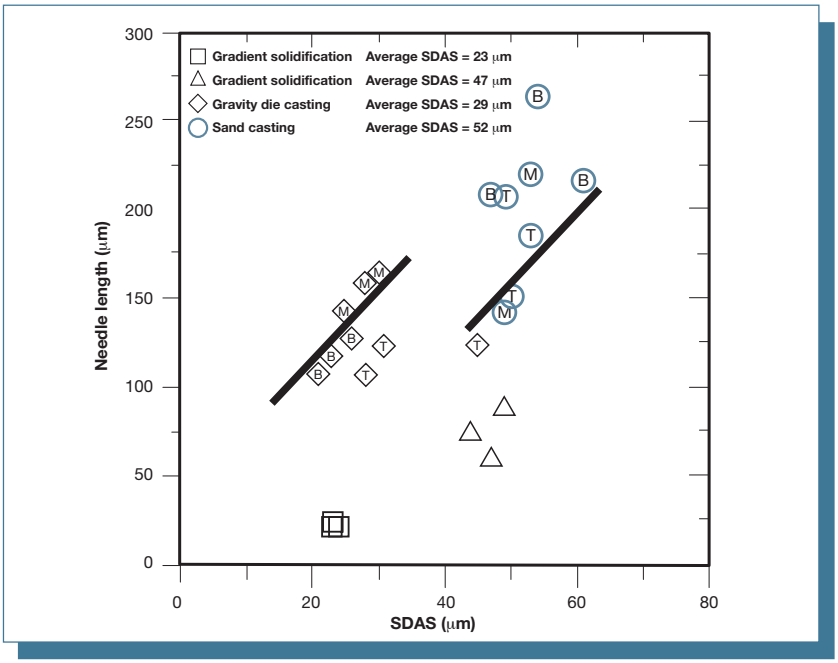


Fig. 10: This graph shows the relation between the β-phase length and the SDAS.

and their formation reduces the Mg available in the melt to form $Mg_2Si$ which has a hardening effect and improves both the yield and ultimate tensile strengths.

Generally, larger SDAS is associated with lower cooling rates and also with longer β-phase needles. The local solidification time influences the growth of the intermetallics that develop and grow during the solidification process, and hence a relation between SDAS and the β-phase length is observed as shown in figure 10.

When a tensile sample contains pores it is reasonable to assume that the region of porosity will yield first due to the reduced load bearing area concentrating the stress near the voids. The area fraction of porosity was determined by measuring the area just below and at the fracture surface. The first mentioned was measured by an image analyzer and the latter was photographed and observed by scanning electron microscopy, SEM. This method enables an examination of the distribution and size of the pores.

In the present study, it has been observed that the cooling rate, SDAS in this case, seem to govern the length as well as the percentage area fraction of porosity to some extent, see figure 11. It appears that a reduction in SDAS results in smaller average pore size and a reduced area fraction of porosity. It is obvious that as the solidification time is low, less time will therefore be available for the diffusion of the hydrogen into the interdendritic regions which results in small sizes and fraction of pores. But comparing the porosity formation, the gradient solidified samples with SDAS ~ 23 μm are associated with largest percentage area fraction of porosity which might be due to the arrestment of premature pores as they become entrapped by the advancing solidification front.

The discrepancy could be derived from the theory that involves the harmfulness of the oxide films, which suggests that when an oxide particle is approached by the solidification front, the particle experiences the hydrogen-rich environment produced by the rejection of gas from the advancing solid. Furthermore, the access of gas by diffusion into the air pocket in the gap of the oxide particles, the pore will start to form and grow. As the freezing rate is slow and the particle is poorly wetted by the melt, time will therefore be available for more hydrogen to diffuse resulting in pore expansion and growth.

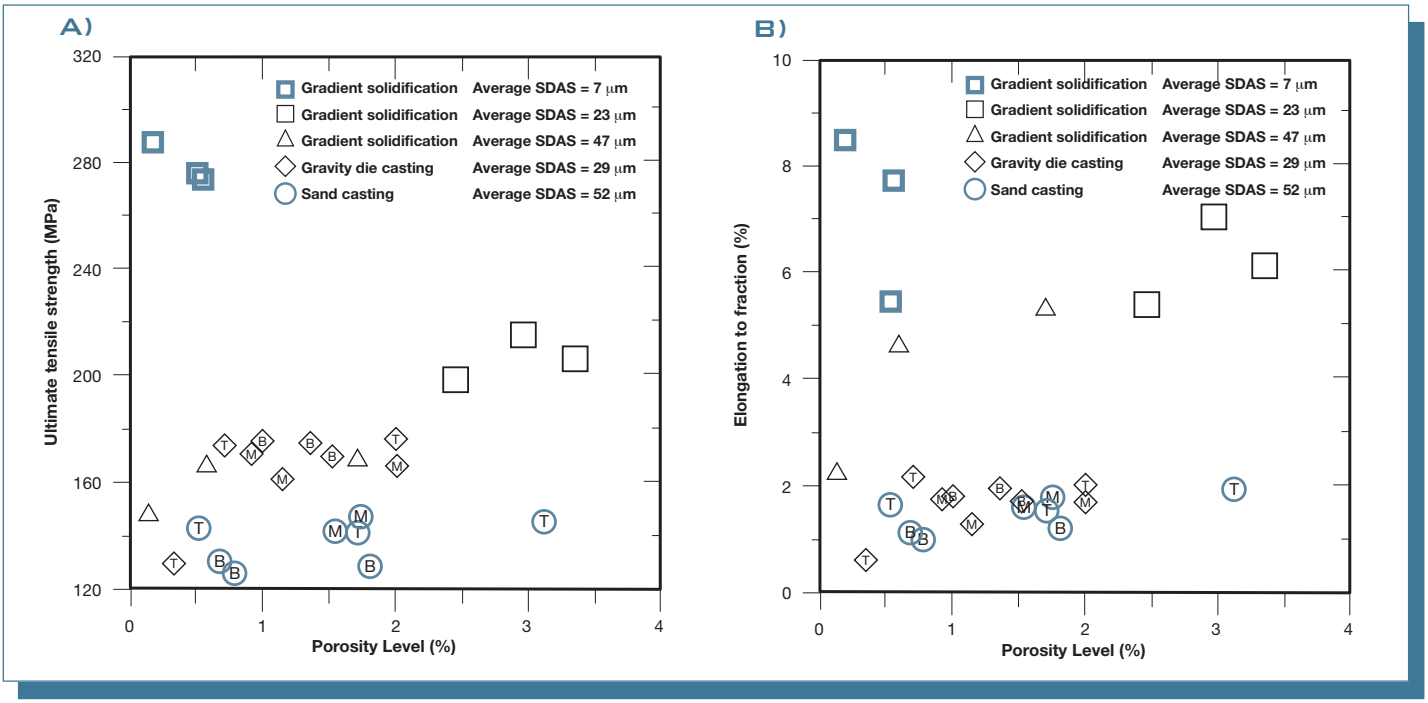


Fig. 11: The graphs a) and b) illustrate the influence of porosity on the tensile properties.

In the case of the larger SDAS ~ 47 μm, it is therefore reasonable to assume that due the slow cooling conditions many air pockets formed within the liquid or due to interaction with oxide particles have been driven in front of the solidified front without being engulfed and in that case not been detected in the gradient solidified specimens due to the solidification mode. Another reason might be the longer time available for the hydrogen to diffuse and move in front of solid-liquid interface out of the sample into the surrounding environment.

The scatter in the data is too great to derive any clear correlation between porosity level and the tensile strength and ultimate elongation, see figure 11 a and b. According to literature, it is stated [2] that the static tensile properties such as ultimate tensile strength, yield strength and elongation to fracture, were all decreased with an increased degree of porosity. On the contrary, according to [3-7], the reduction in tensile properties has almost no correlation with the average volume fraction of porosity. In fact, the decrease in tensile properties was attributed to the length and/or the area fraction of defects in the fracture surface. Development of a high fraction of porosity may also be due to Fe in the melt. The long, needle-shaped iron intermetallic phase formed is expected to cause severe feeding difficulties during solidification. The morphology of the β-phase blocks the interdendritic flow channels, which is why it is proposed that higher iron contents in the alloy are associated with higher levels of porosity.

SEM examination was also performed in order to study what kinds of pores are frequently found on the fracture surfaces in this work. Figure 12a illustrates a pore seen in a sand cast specimen and 12b is seen in a gradient solidified specimen at a solidification rate of 3 mm/s.

Worth to indicate is that the melt hydrogen content has not been measured and assumed in this case to be constant for all the alloys since they have been produced under similar conditions.

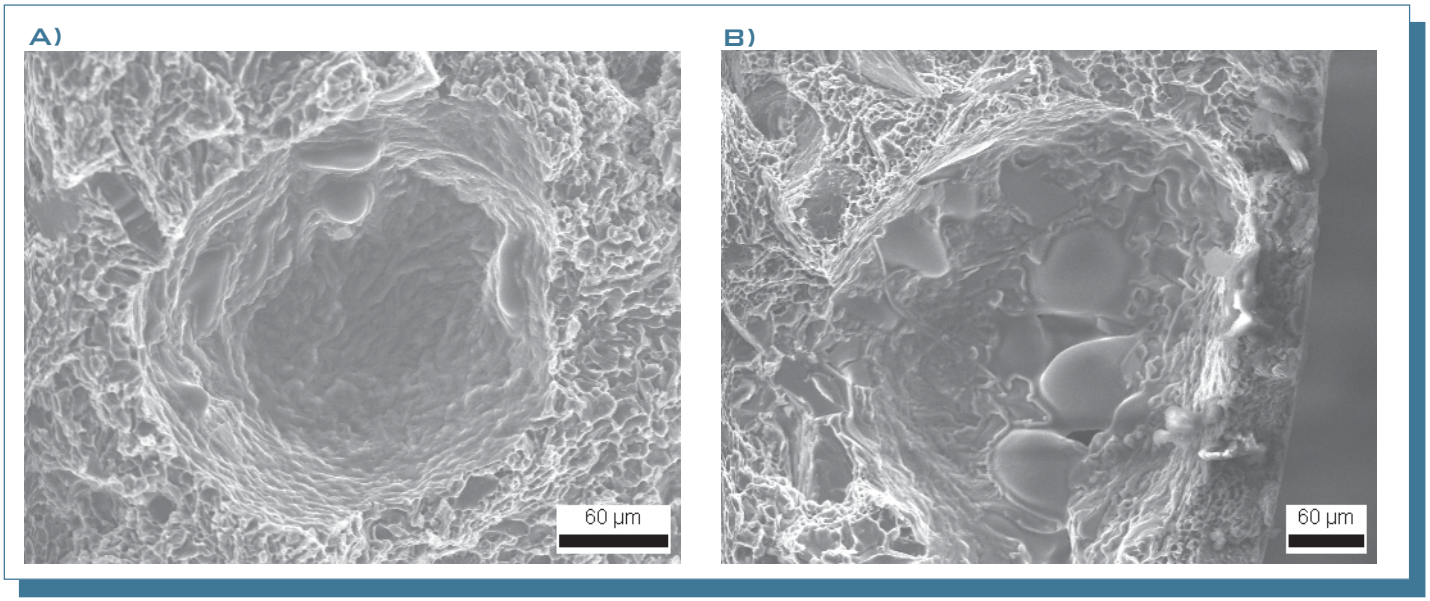


Fig. 12: Illustration of pores. a) Showing sphericity of a possible gas pore b) The cavity is observed at the edge of the fractured surface shows a possible gas-shrinkage pore.

## DISCUSSION

Generally, the mechanical properties of metals are widely influenced by their microstructures. When defining the microstructure many parameters have to be taken into account, and these include among others the secondary dendrite arm spacing, the size and shape of precipitated phases such as silicon and iron-bearing phases, grain size, porosity, etc.

In this investigation, many of the parameters mentioned above have been measured and correlated to the mechanical properties. Constituents that may have deleterious effect on the mechanical properties are defects such as oxide films or undesired phases and inclusions.

A comparison of the results of the tensile testing with the casting method and the corresponding specimens with three different solidification rates obtained by gradient solidification shows clearly that the tensile behaviour and production method is related by three different stress-strain curves. The material exhibiting SDAS ≈ 7 μm results in the highest stress-strain combinations as shown in the diagram in figure 13. The main reason for this behaviour is the finer microstructure, a more homogeneous distribution of the intermetallic phases and lower levels of porosity. Even though there are no specimens with corresponding SDAS extracted from commercial components available in this study, this data clearly shows the inherent potential strength of the alloy.

The stress-strain values for the sand cast specimens follow the curve for SDAS = 47 μm (obtained by gradient solidification), but fracture occurs at lower stress and strain levels, see figure 13. The stress-strain curve for SDAS = 23 μm (by gradient solidification) corresponds well to the stress-strain values of the gravity die cast specimens.

The reason why the sand and gravity die cast specimens fractured much earlier than the gradient solidified specimens, and exhibited different

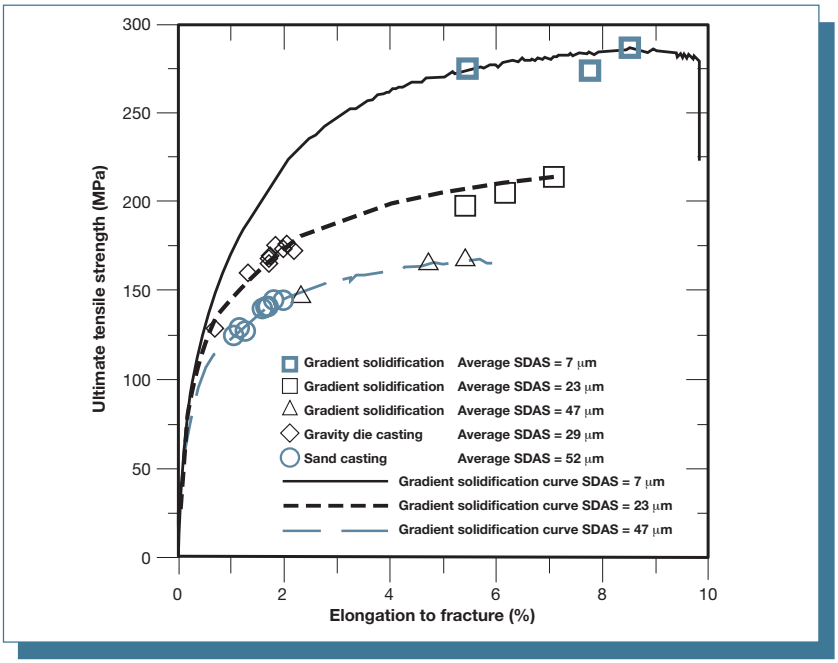


Fig. 13: This graph shows tensile test curves for the gradient solidified specimens and includes mechanical properties data for the gravity die and sand cast specimens.

combinations of strength and fracture elongation values may be due to the formation of brittle and coarse intermetallics such as the iron-bearing β-phase and an inhomogeneous microstructure. Even if similar SDAS has been obtained from the gradient solidification equipment, the variations in the β-phase needles, local coarsenesses of microstructures and sizes of intermetallics are likely to be different due to microsegregation in the castings. Segregation of elements is likely to occur in castings and this will affect the development and solidification sequences of the microstructure and lead to local variations in mechanical properties. At the thinner part of the fan blades the β-phase needles are likely to be short and have no time to grow and coarsen as is the case in thicker parts where the local iron level might also be different. It has also been shown that a finer microstructure with smaller SDAS is beneficial for the mechanical properties. A finer microstructure means larger areas of grain boundary leading to more difficulties for continuation of slip and dislocation movement during deformation, hence yielding stronger alloys. A simple tool that might be used to predict the impact of changes in the chemical composition, solidification rates and routes, microstructure and heat treatment on the tensile performance is by implementing a quality index, Q. Its practical value originates from the fact that the mechanical "quality" of an alloy is expressed by a single numerical parameter, whose value can be read off a quality index chart or calculated through a simple equation relating the elongation to fracture, $s_f$, the ultimate tensile strength, UTS, and d, which is an empirical parameter chosen to be around 150 MPa for EN AC 43100 (Al-7%Si-0.4%Mg) to make Q more or less independent of the yield strength of the alloy, as seen in equations 1-2, [8-10]:

$$Q = UTS + d * \log (100 * s_f) \quad (1)$$

$$\sigma = K\varepsilon^n \quad (2)$$

where σ is the true flow stress, *K* is the alloy's strength coefficient, $\varepsilon$ is the true plastic strain and *n* the strain hardening exponent.

In order to produce the charts in figure 14, a mean value for the strength coefficient, K, has been calculated. For the commercial cast components, figure 14a, K is approximately 410 MPa and for the gradient solidified materials K is around 430 MPa, figure 14b. The strain hardening exponent, n, is numerically equal to the necking onset strain

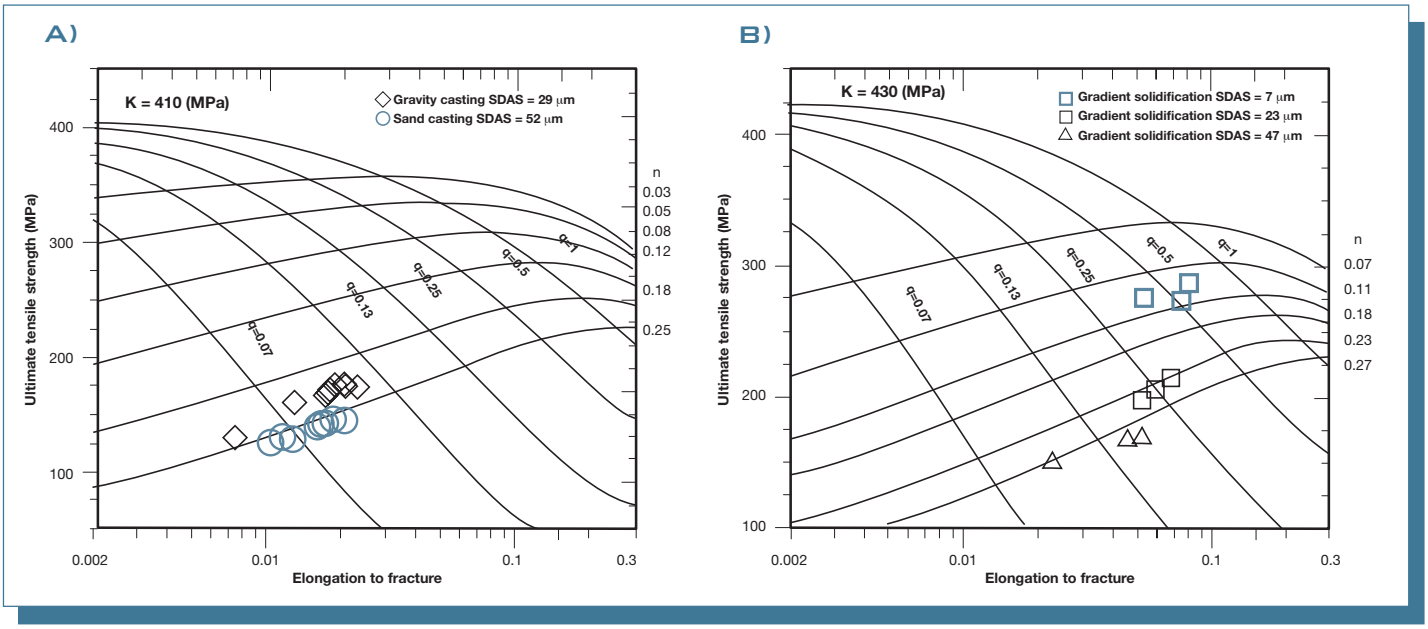


Fig. 14: A quality index chart for the alloy studied obtained for gravity- and sand cast samples is presented in a) while b) represents the gradient solidified specimens. The mean value of the strength coefficient is a little higher for the gradient solidified specimens.

and can be used to define the relative ductility parameter, q, see equation 3.

$$q = s_f / n \quad (3)$$

Defining q = 1 means the onset of necking represents samples that fail either at the onset of necking or beyond, while q < 1 identifies lower quality or less ductile samples. For instance q = 0.5, 0.2, 0.1 identifies samples that fail at 50%, 20% and 10% of their maximum uniform strain, respectively.

As observed, the points corresponding to SDAS = 52 μm are located near the bottom of the chart, which may be due to their coarser microstructure and the length of the β-phase. As the strength of the gravity die cast specimens increases, the data points shift toward the upper right corner.

Regarding the gradient solidified samples, the data points for the SDAS = 7 μm specimens, with the finer microstructure, exhibit the highest values of Q and q. These values seem to be the only ones that reach the limit imposed by the necking line q = 1.

As the SDAS and the level of deleterious microstructural compounds are decreased, the strength and ductility of the alloy is increased and so does the Q, allowing for a possible comparison between different alloys and processing routes. Furthermore, the Si particles, playing a role as reinforcing phases, decrease in size and the shape becomes more fibrous, which has an overall beneficial effect on the mechanical properties.

## CONCLUSIONS

As an outcome from the current investigation, the dendritic cell size, SDAS, and the length of iron-bearing phase whether as needles or Chinese script, governs the tensile strength and ductility of Al-Si-Mg alloys. The early fracture of sand and gravity die cast specimen can be related to the length of the iron-bearing phase, oxide films entrapment, and inhomogeneous microstructure and to the Si particle size and morphology, which determine the rate of particle cracking with the applied strain.

- A finer microstructure, small and well distributed iron-rich compounds and low levels of porosity exert a beneficial impact on the resulting mechanical properties.
- The locally increased levels of iron due to possible segregations might have resulted in longer and larger fractions of β-phase needles. The main reason for the remarkable reduction of the mechanical performance of commercial components is proposed to be due to the presence of the locally induced stresses by the needles which break, link and propagate the cracks in an unstable manner. The higher the solidification rate the shorter the length of the needles and the sounder the material.
- The gradient solidification method shows that the EN AC 43100 alloy used for commercial cast components processed by sand and gravity die casting, has an *improvement potential* to provide sounder castings with substantial ductility.
- The addition of Mn did not alter the morphology of iron-bearing β-phase into a more compact Chinese script. Instead, these iron intermetallics seem to be coexisting in the microstructure.
- Porosity is not found to be the primary parameter controlling the tensile strength and ductility, but it is worth bearing in mind that the reduction of the load bearing area generally has a harmful influence on the overall properties.

## ACKNOWLEDGEMENTS

The authors acknowledge Johan and Jan Tegnemo at Mönsterås Metall AB for their invaluable help and support for making the experiments in the foundry and Nordic Industrial Fund for the financial support within the Nordic Project STALPK.

## REFERENCES

1. *Metals Handbook;* ASM International, 1998, pp. 663-665.
2. M. Avalle, G. Belingardi, M.P. Cavatorta and R. Doglione, *International Journal of Fatigue Vol. 24* , (2002), pp. 1-9.
3. C.H. Cáceres and B.I. Selling , *Materials Science and Engineering A,* Vol. 220, Issues 1-2, (1996), pp. 109-116.
4. M. Harada, T. Suzuki and I. Fukui , *Journal of the Japan foundrymen´s society* Vol. 55, No. 12, (1983), pp. 47-50.
5. M.K. Surappa, E. Blank and J.C. Jaquet, *Scripta Metallurgica*, Vol. 20, No. 9, (1986), pp. 1281-1286.
6. J.G. Conley, J. Huang, J. Asada and K. Akiba, *One Hundred Third Annual Meeting of the American Foundrymen's Society*; Rosemont, IL; USA, (1998). pp. 737-742.
7. C.H . Cáceres, *Scripta Materialia* Vol. 32 No. 11, (1995), pp. 1851-1856.
8. C.H. Cáceres, I.L. Svensson, J.A. Taylor, *International Journal of Cast Metals Research*, Vol. 15, No. 5, (2003), pp. 531-543.
9. C.H. Cáceres, *International Journal of Cast Metals Research*, Vol. 12, (2000), pp. 367-375.
10. M. Drouzy, S. Jacob and M. Richard, AFS *International Cast Metals Journal*, Vol. 5, No. 2, (1980), pp. 43-50.